Geomechanics and Engineering, *Vol. 40, No. 4 (2025) 277-293*
https://doi.org/10.12989/gae.2025.40.4.277

Bearing pressure enhancement of sand foundation beds by encapsulating geogrids in thin densified gravel layer inclusions

S.N. Moghaddas Tafreshi*[1], H. Alizadeh Balf[1a],
H.R. Rezaeinejad[1b], B.C. O'Kelly[2c] and A. Faramarzi[3d]

[1]*Department of Civil Engineering, K.N. Toosi University of Technology, Tehran, Iran*
[2]*Department of Civil, Structural and Environmental Engineering, Trinity College Dublin, Dublin, Ireland*
[3]*School of Engineering, University of Birmingham, Birmingham, UK*

(*Received June 14, 2024, Revised January 14, 2025, Accepted Februaryr 12, 2025*)

Abstract. This paper presents a novel experimental investigation for improving the bearing pressure resistance of medium-dense sand deposits. Model footing tests were performed on similarly prepared sand beds to examine the effects of incorporating one, two and three separate geogrid-reinforced thin densified gravel layers at various depths within the beds. Additional load tests investigated incorporating only geogrid-reinforcement layers or densified gravel layers of different thicknesses placed separately within the sand beds for the purposes of establishing their resistance contributions. Furthermore, a dimensional analysis relating the model test results to the large-scale conditions is presented. Compared to the unreinforced medium-dense sand bed, superior bearing-pressure resistances (and reduced footing settlements) were achieved for including the geogrid-reinforced gravel layers. For example, at a settlement ratio of 2% (s/D = 2%), the inclusion of one, two, and three geogrid-reinforced thin densified SwG layers improved performance by 68%, 110%, and 124%, respectively, compared to the unreinforced sand bed. Increasing the number of these layers (from one to three) produced improved geomechanical performance, albeit more layers produced diminishing returns. The basic mechanisms responsible for the improvements in bearing pressure resistance are elucidated. This study demonstrates that when suitable engineering fill is unavailable, the concept of incorporating geogrid reinforced thin densified granular layers in the backfill could be of practical application for constructing reinforced footings, reinforced soil walls, etc.

Keywords: bearing capacity; geogrid; settlement; thin sand layer; uniform sand

1. Introduction

The construction of structures and roads on soil deposits with inadequate bearing-pressure resistance (i.e., such that they may undergo excessive settlements) is one of the major challenges in geotechnical engineering practice. For instance, in many areas of the world, aeolian sand deposits can present geoengineering challenges in terms of comparatively low allowable bearing pressures. Typically, for coarse-grained soils, ground improvement by densification, employing vibratory or dynamic compaction techniques, can be considered, although high-quality compaction of loose uniform sand deposits may prove difficult or ineffective. For instance, aeolian sand grains typically have a rounded particle shape that can affect their ability to interlock during the compaction process, which, along with the absence of fines (i.e., silt/clay content), inhibits the formation of a stable structure under compaction forces. Furthermore, the moisture content plays a crucial role in achieving optimal compaction — overly dry conditions hindering the compaction effort, whereas an excessive water content makes it difficult to achieve the targeted compaction density. Hence, alternative ground improvement techniques must be considered, that could include the soil replacement method, soil reinforcement using geosynthetics, other structural inclusion types (e.g., stone columns or piles), and various chemical soil stabilization applied by mixing or grouting techniques. Amongst these approaches, soil replacement and geosynthetics reinforcement are often considered as simple ground improvement strategies. However, the replacement of a significant volume of inferior soil with high-quality soil may prove uneconomical, while the inclusion of thin densified coarse-grained soil layers mobilising high shear strength may not fully meet the necessary bearing capacity requirements for the foundation bed. Geotextiles, geogrids, geocells, fibers, etc. have proved their worth in a vast number of projects, with applications including the enhancement of the bearing pressure of foundation beds (Biswas and Krishna 2018, Biswas and Mittal 2017, Tolun *et al.* 2021, Moghaddas Tafreshi *et al.* 2022, Liu *et al.*

*Corresponding author, Professor
E-mail: nas_moghaddas@kntu.ac.ir
[a]Former MSc Student
E-mail: hassanalizadeh1997@gmail.com
[b]Former MSc Student
E-mail: h2rn97@gmail.com
[c]Associate Professor
E-mail: bokelly@tcd.ie
[d]Professor
E-mail: a.faramarzi@bham.ac.uk

ISSN: 2005-307X (Print), 2092-6219 (Online)

2024), railways and roads (Khalaj *et al*. 2015, Moghaddas Tafreshi *et al.* 2021, Punetha and Nimbalkar 2022, Zhao *et al.* 2023), buried structures (Pires and Palmeira 2021, Giroud et al. 2023) and embankments, slops and retaining walls (Altay *et al*. 2021, Yazdani and Ashtiani 2023, Ouyang *et al.* 2024, Tarraf and Seyedi Hosseininia 2024, Liu *et al*. 2024). Extensive studies have investigated the beneficial role of planar inclusions in soil using geotextiles or geogrids (O'Kelly and Naughton 2008a, b, Ok *et al.* 2023). However, the efficacy of soil reinforcement for weak clay and loose sand may be constrained by the low shear resistance developed along the soil–geosynthetic-layer interface, such that the tensile capability of the reinforcement layer may not be sufficiently mobilized for contributing adequately to resisting the applied ground loading. An integrated approach can be adopted to overcome this limitation and to provide a more effective and economical solution overall, i.e., one that applies both the soil replacement and geosynthetics reinforcement strategies. In other words, the geosynthetic reinforcement layer(s) are embedded in thin densified layer(s) of replaced coarse-grained soil that are constructed within the weaker main soil deposit. For instance, this approach could take the form of separate geogrid reinforcement layers, each embedded in a thin densified gravel layer, and which are incorporated at various depths within a medium-dense uniform sand deposit. The described scenario is investigated in the present research for improving the bearing pressure resistance in response to a circular footing load applied at the ground surface.

Geosynthetic reinforced soil has been extensively investigated using direct-shear and pullout tests (Abdi *et al*. 2009, Abdi and Arjomand 2011, Abdi and Zandieh 2014, Zhao *et al.* 2024, Roy *et al.* 2024). For instance, Abdi *et al*. (2009) performed large-scale direct-shear tests to investigate the soil–geogrid interaction for the clay–geogrid, sand–geogrid and clay incorporating thin geogrid-reinforced sand layer scenarios. Abdi and Arjomand (2011) and Abdi and Zandieh (2014) conducted a series of pullout tests to investigate the geogrid reinforcement of clayey soil, with/without the geogrid layer encapsulated within a thin sand layer. Furthermore, Abdi *et al*. (2019) reported on the significant influences of (a) the ratio between the soil particle and geogrid-aperture sizes, and (b) the thickness of the geogrid's transverse elements on the mobilized pullout resistance, with superior soil–geogrid interaction achieved for the geogrids encapsulated within thin sand layers. Based on the results of triaxial compression testing for 100-mm dia. specimens, Ahmadian and Moghaddas Tafreshi (2020) recommended incorporating geotextile layers encapsulated within sand lenses to improve the shear strength of fine sand. They emphasized that incorporating geotextile layers within competent sand lenses contributes to increased frictional interaction between the geotextile surfaces and surrounding soil, resulting in the superior geomechanical performance of the test specimens. Ghiassian and Jahannia (2004) investigated the load bearing pressure–settlement response of geogrid-reinforced clayey soil. Due to insufficient interface friction between the clayey soil and geogrid layer, they incorporated a thin sand layer that encapsulated the geogrid layer, for the purposes of mobilizing larger tensile resistance forces along the geogrid layer. Overall, therefore, using the thin coarse-grained soil layer and geosynthetic layer combination within a clayey deposit can enhance the shear resistance of the foundation bed system in a tailored way. In other words, the incorporation of the thin geogrid-reinforced coarse-grained soil layer(s) increases the tensile strength of the clayey soil mass, thereby reducing the deformations in the subsoil and enhancing the overall bearing capacity of the foundation bed system. Additionally, compared to the bulk soil-replacement approach, incorporating thin geogrid-reinforced coarse-grained soil layer(s) within the clayey foundation bed necessitates smaller quantities/volumes of high-quality geotechnical materials (i.e., coarse-grained soil and geosynthetic materials) to achieve the required foundation bed properties.

Research has shown that due to insufficient interface friction between clayey soil and the geogrid layer, using a thin sand layer to encapsulate the geogrid can improve the pullout resistance of geogrid reinforcement in clayey soil (Abdi *et al*. 2009, Abdi and Arjomand 2011, Abdi and Zandieh 2014). This technique has also been studied for enhancing the pressure–settlement response of geogrid-reinforced clayey foundation bed (Ghiassian and Jahannia, 2004). However, there remains a gap in research regarding the improvement of the bearing capacity of loose and medium-dense sand deposits (e.g., aeolian sand), which are difficult to compact or densify using conventional vibratory or dynamic compaction techniques. Thus, the present research investigates the scenario of improving the bearing pressure resistance of medium-dense uniform sand foundation beds by incorporating thin geogrid-reinforced densified gravel layers at various depths within the beds. For this scenario, the uniform sand at the construction site location may not possess the required qualities (of particle grading and friction angle) for generating adequate interface frictional resistance with the embedded geogrid layer, such that the geogrid-reinforced sand deposits may still have a comparatively low allowable bearing pressure. With its higher internal friction angle, the introduced densified gravel material that fully encapsulate the geogrid layers can generate superior interface frictional resistance, thereby mobilizing larger tensile resistance force along the geogrid layers, with the overall effect of enhancing the stability of the foundation bed system and reducing the deformations in the subsoil. The reduced-scale model footing tests presented herein investigates the performance benefits of incorporating one, two or three separate geogrid-reinforced thin densified gravel layers on the bearing pressure resistance and settlement response of medium-dense uniform sand beds when subjected to monotonic vertical loading of a circular footing placed centrally on the sand bed surface. These results are compared with those achieved for similarly prepared sand beds incorporating only geogrid-reinforcement layers or thin densified gravel layers. Additionally, the effect of the thickness of the introduced densified gravel layer(s) on the mobilized bearing pressure resistance versus settlement behavior of the medium-dense sand beds was examined. The basic

Fig. 1 Clean, medium-sized silica sand (*left photo*) used for preparing the medium-dense soil beds and well-graded SwG soil (*right photo*) used in forming the thin densified coarser layers incorporated within the sand beds

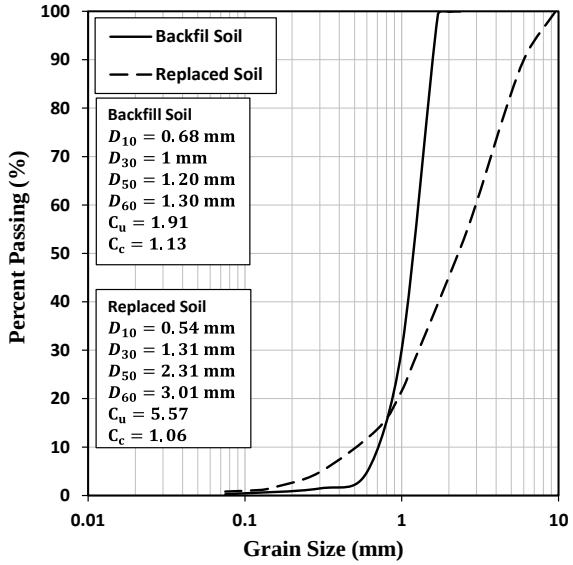

Fig. 2 Particle-size distributions of the silica sand and SwG materials used in forming the soil beds and thin densified layers, respectively

mechanisms responsible for the mobilized bearing pressure resistances, and their enhancement factors (in terms of the relative bearing pressure resistance increases compared to that of the unreinforced sand bed), are determined for these different soil improvement strategies. Additionally, the authors present a dimensional analysis for relating the presented model test results to the large-scale field conditions.

2. Material properties

This study employed two clean coarse-grained soils, namely a medium-sized silica sand (soil A, sourced from Firuzkuh, Iran) and a well-graded sand-with-gravel (SwG) soil (i.e., soil B). Fig. 1 shows a photograph comparing the appearance of the two soils. As described later (in section 5), the model footing tests involved load testing medium-dense soil beds prepared using soil A, which incorporated up to three thin unreinforced or geogrid-reinforced densified SwG layers. Soil A was a relatively uniform silica sand of rounded grain sizes with a particle-size distribution in the range of 0.085–1.7 mm, and a mean grain size of D_{50} = 1.2 mm (see Fig. 2). This soil had measured maximum and minimum void ratio values of 0.85 and 0.61, respectively. Triaxial compression testing of dry soil A specimens prepared at a relative density of D_r = 58% (i.e., at the same D_r value as the sand beds tested in the model footing experiments) indicated an internal friction angle of ϕ = 32.5°.

Soil B with granular particles had a mean grain size of D_{50} = 2.3 mm, a maximum grain size of 10.0 mm (see Fig. 2), and its specific gravity of solids value was G_s = 2.65. Modified Proctor (MP) compaction (ASTM D1557-12) of

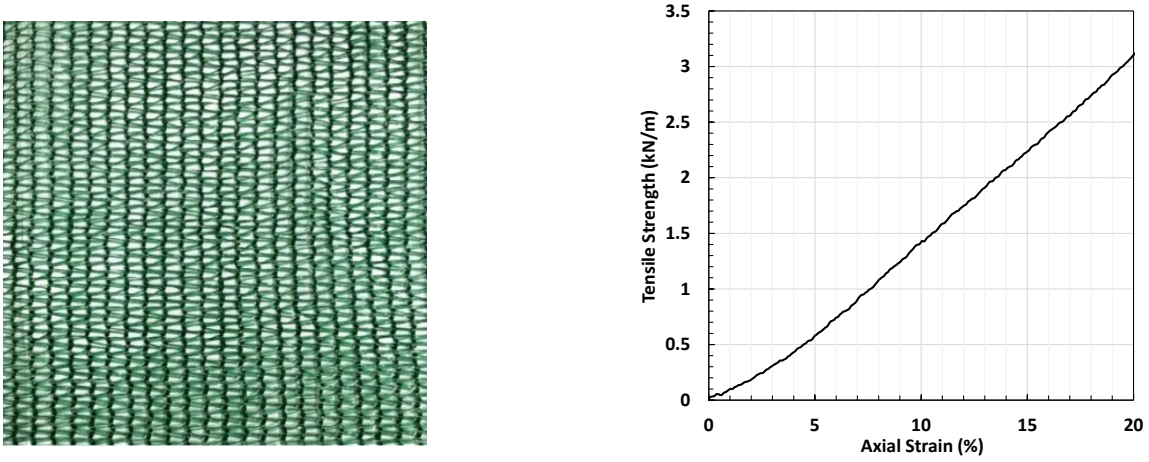

(a) (b)

Fig. 3 Geogrid reinforcement material: (a) image of the specific geogrid; (b) variation of its tensile resistance (per meter width) against axial strain

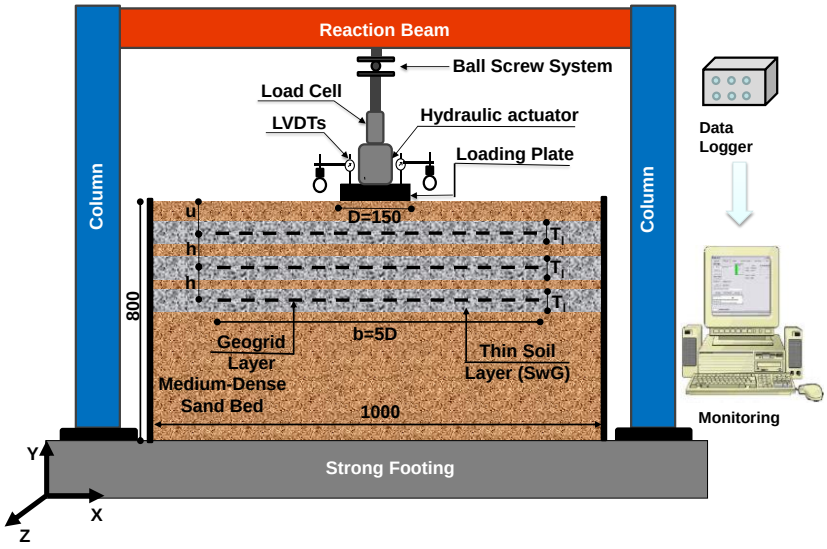

Fig. 4 Schematic view of the model test set up (units in millimetres: not to scale)

the soil B material produced a maximum dry unit weight (MDUW) of 19.52 kN/m^3, achieved at a moisture content of 6.7%. Consolidated-drained triaxial compression testing indicated an internal friction angle of ϕ = 37.5° for a relative compaction of R_c = 90% (MDUW of 17.57 kN/m^3), i.e., at which the thin densified SwG layer(s) were formed within the sand beds.

A single geogrid type was used for the reinforcement layer(s) formed within the sand beds. Fig. 3 shows an image of the geogrid, along with its measured tensile stress–strain behavior. As elaborated later in section 7, the low tensile strength of the geogrid reinforcement used was to account for scale effects associated with the model footing tests. In fact, because of its fine network structure and low tensile strength, the geogrid behaved more like a geonet. The geogrid material (0.965-mm in thickness, t) was made of polyester yarns woven with triangular-shaped apertures, with the largest aperture size of 3 mm, a unit weight of 150 g/m^2, and tensile force resistances of 0.10, 0.58 and 1.43 kN/m mobilized at 1%, 5% and 10% strains, respectively.

3. Experimental setup

Fig. 4 presents a schematic cross-section of the model footing test arrangement. The soil foundation was prepared to fill the 1.0-m square (in plan) × 0.8-m-deep test chamber. For illustration purposes, the medium-dense sand bed (of soil A material) is shown to incorporate three separate thin densified SwG layers, each shown to encapsulate a geogrid reinforcement layer. However, as described later, soil beds incorporating 0, 1, 2 or 3 thin densified SwG layers, with/without geogrid reinforcement included, were investigated for the testing program presented in this paper. Three sides of the test chamber were made of 20-mm thick, high strength medium-density fiberboard (MDF) sheets, while the fourth side was made of transparent dense plastic (Plexiglas) for observation and potential imaging of the placed soil beds. Stiff steel profiles fitted around the outside perimeter of the test chamber restrained undesirable outward movement/bulging of its sidewalls (i.e., rigid lateral boundary condition), which was confirmed by

Table 1 Testing program for investigating the effects of geogrid reinforcement, thin densified SwG layers, and their combination within medium-dense sand beds (b/D = 5 and u/D = h/D = 0.33)

Test series	Reinforcement type	No. of geogrid layers (N_{gr})	No. of densified SwG layers (N_{dl})	Thickness of SwG layers (expressed as T_l/D)	No. of tests
1	Unreinforced	0	0, 1, 2*, 3*	0.20	4+2 (repeated)
2		0	1*	0.13, 0.26	2+1 (repeated)
3	Geogrid- reinforced	1, 2, 3**	0	0	3+2 (repeated)
4		1	1	0.20	3+2 (repeated)
		2**	2**		
		3	3		
5		1*	1*	0.13, 0.26	2+1 (repeated)

To verify repeatability of results, tests marked "*" were performed twice and those marked "**" were performed thrice

insignificant outward movement (<1 mm) measured by horizontally mounted linear-variable displacement transducers (LVDTs) contacting with the outside faces of the chamber sidewalls. A 150-mm diameter (D) by 20-mm-thick steel plate was used to apply a vertical load centrally to the soil bed surface. Note, as the chamber's width (length) of 1.0 m was about seven times greater than the loading plate diameter, it was safe to assume that there was no sidewall-effect interfering with the footing's load–deformation results (Sireesh *et al.* 2009). This assumption was verified in some of the tests reported here (both reinforced and unreinforced), through horizontal observations via the plexiglas and vertical measurements. In these tests, it was found, by using a straight edge to identify the soil areas unaffected by heave, that the soil surface exhibited no visible bulging beyond approximately 4.5 and 3.5 radii from the loading axis for unreinforced and geogrid-reinforced beds, respectively. For reinforced beds, the boundary of the affected soil always remained within the reinforced zone. These findings provide confidence that the boundary effect of the testing tank walls on the results was probably insignificant, even at the largest settlements, for all tests, considering that the box wall is located about 7 times the load plate radius from the loading axis.

The footing loading system was comprised of a vertically mounted 10-kN-capacity hydraulic actuator, secured to a stiff horizontal reaction beam located above the test chamber, along with a control unit for regulating and recording the actuator pressure. The applied footing load was measured using an *S*-shape load cell with an accuracy of ±0.01%. Two 50-mm-stroke LVDTs, each having an accuracy of ±0.01%, measured the footing's settlement response. All the measuring devices were recorded via a 16-channel analog-digital data logger/control unit. To assess the readings' accuracies, all these devices were calibrated before commencing each test series, achieved by comparing their readings with those of other devices with known calibration factors. As the footing's load–settlement behavior is of utmost importance for the designer and researchers, and because of the limited number of instruments available in performing the present investigation, only the applied footing load and settlement response were measuring using the load cell and LVDTs. However, the use of other instrument types (e.g., soil pressure cells and strain gauges), which were not available for inclusion in this testing program, would have been beneficial. They could be used in a future study to evaluate the effect of the proposed reinforcement strategy of incorporating thin geogrid-reinforced densified SwG layers on the patterns of stress and strain transferred through the soil beds.

4. Model geometry and test program

The research objectives of the testing program were to assess the impact on the footing's bearing pressure–settlement behavior of incorporating geogrid-reinforcement and thin densified SwG layers in medium-dense sand beds. In other words, footing tests were performed on uniform sand beds incorporating the geogrid layer(s) alone, thin densified SwG layer(s) alone, and their combination. Another objective was to assess the impact of the thickness of the densified SwG layer(s) on the footing's bearing pressure–settlement behavior.

Table 1 summarizes all the testing performed, comprising of five test series. The investigated number of geogrid reinforcement layers (N_{gr}) and thin densified SwG layers (N_{dl}) both ranged between zero and three. Referring to Fig. 4, the placement depth (u) to the center of the uppermost (first) geogrid layer, and the vertical spacings (h) between the neighboring geogrid layers, are expressed in non-dimensional form with respect to the footing diameter (i.e. as ratios of u/D and h/D). In the present investigation, the ratios u/D and h/D were set at their optimum values of 0.33 (Moghaddas Tafreshi and Dawson 2010). It should be noted that the optimum location of the upper layer of reinforcement (u/B) can vary in multi-layer reinforcement systems. Abu-Farsakh *et al*. (2007) conducted a finite element study on geogrid-reinforced silty clay soil beds and found that while the bearing capacity dependence on the depth ratio (u/B) is similar across single-layer, two-layer, and three-layer reinforcement systems, the u/B value tends to decrease slightly with an increasing number of reinforcement layers. They reported that the optimal u/B value varies from 0.4 in single-layer systems to 0.3 in three-layer systems. Additionally, according to the findings of Moghaddas Tafreshi and Dawson (2010), the square area

(i.e., $b \times b$) of the embedded geogrid layers was held constant in all the tests at $b = 5 \times D$. Whereas the SwG layer(s) covered the entire plan area of the test chamber. The thickness (T_l) of the SwG layers is also expressed in non-dimensional form with respect to the footing diameter, with selected T_l/D values of 0.13, 0.20 and 0.26.

Referring to Table 1, test series 1 investigated the case of the sand beds incorporating N_{dl} = 0, 1, 2 and 3 densified unreinforced SwG layers, with T_l/D selected as 0.20. Test series 3 investigated the case of the geogrid-reinforced sand beds without any SwG layers, i.e., N_{gr} = 1, 2 and 3, with N_{dl} = 0. Test series 4 investigated the combined case of the geogrid reinforcement encapsulated within the SwG layer(s); i.e., for $N_{gr} = N_{dl} = N_{gr\text{-}dl}$ = 1, 2 and 3. Test series 2 and 5 were conducted to investigate the effect of varying the thickness of a single unreinforced and geogrid-reinforced SwG layer on the footing's bearing pressure–settlement response, considering the cases of T_l/D= 0.13, 0.20 and 0.26. Overall, 14 independent tests were performed, along with eight repeat tests demonstrating the experiments repeatability. The repeat tests indicated a maximum ~2–4% difference between the results obtained for notionally identical tests, confirming the good repeatability/dependability of the results. The tests were repeated two or three times as specified by "*" and "**" in Table 1, respectively.

5. Preparation of the soil test beds

While the dense state is preferred in the field conditions, as described in the Introduction, certain types of loose and medium-dense sand deposits (e.g., aeolian sand) can prove difficult to compact/densify using conventional vibratory or dynamic compaction techniques. Hence, an alternative ground improvement proposal is investigated in the present study, whereby thin geogrid-reinforced densified gravel layers are introduced into the medium-dense sand beds. Accordingly, the air-pluviation (raining) technique was used to deposit layers of the dry sand (soil A) in the test chamber at a known and uniform density. A moveable steel hopper, 300-mm square (in plan) by 450-mm high, was positioned directly above the empty test chamber, with adjustment of its elevation to control the sand drop height. A simple sliding system (of a perforated plate in the hopper's funnel outlet) controlled the start or stop of the sand raining process. The sand flow rate was regulated by fitting perforated plates with different aperture sizes. Before using the hopper for depositing the sand layers in the test chamber, the pluviation technique was calibrated (necessitating the determination of the required sand raining height and flow rate) to consistently produce uniform sand layers at the targeted relative density of D_r = 58% (void ratio to 0.75). In these calibration trials, the dry sand exited the hopper through different perforated plates (investigating a range of aperture sizes) and was allowed fall through various drop heights to fill small cuboidal receiving containers. By weighing the sand-filled containers, the densities of the deposited dry sand for the different depths of the receiving containers were determined from simple mass–volume calculations. This facilitated calibration of the experimental set up, in terms of determining the combination of sand flow rate (aperture size in perforated plate), pouring height (measured from the perforated plate elevation to the middle of each deposited sand layer), and deposited layer thickness necessary to produce uniform sand layers with the required relative density. The results of these trials showed that the targeted relative density (of D_r = 58%) was achieved for depositing a 30 to 50 mm deep sand layer by pluviating the dry sand through a drop height of 300–450 mm, with the performed plate in the hopper funnel outlet having of 3- and 4-mm dia. apertures. After depositing each sand layer, its top surface was leveled accurately using a straight edge. For all of the test series 1–5, the described approach was employed to form the uniformly deposited sand layers in the test chamber.

For the tests with thin densified SwG layers incorporated in the sand beds, after reaching the desired levels of the sand formation, thin SwG layers with specified thickness were placed and compacted to achieve a relative compaction of R_c = 90%. Based on the MP compaction test results, which indicated a MDUW of 19.52 kN/m^3 was achieved for a moisture content of 6.7%, the moist SwG material was evenly placed over the full plan area of the test chamber and uniformly compacted to produce 20, 30 or 40 mm (T_l/D = 0.13, 0.2, 0.26) deep layers having an MDUW of 17.57 kN/m^3 (= 0.9 × 19.52). The compaction energy was imparted by dropping a 2.5 kg mass from a height of 305 mm to impact upon a 200-mm-square steel plate positioned on the top surface of the SwG layer that had been placed at 7% moisture content. Knowing the mass of placed SwG material, the targeted MDUW (of 17.57 kN/m^3) for the densified layers was confirmed by simple mass–volume calculations, with the actual layer thickness observed and measured using rulers secured on the outside surface of the Perspex sidewall of the test chamber. For the tests containing geogrid-reinforced thin densified layers, a single geogrid layer was placed at the mid-depth of each densified SwG layer. Additionally, for the tests with geogrid layers but without thin densified layers, the geogrid layers were placed at the desired specific locations (depths) during the formation of the sand beds.

After depositing and levelling the final sand layer, the steel loading plate (model footing) was carefully placed centrally on the sand bed surface, and the related instruments (i.e., load cell and LVDTs) were positioned and adjusted. In all the tests reported herein, monotonic stress-controlled loading was applied to the footing at a constant rate of 1.5 kPa/s. The applied footing load and its settlement response were continuously recorded using the data acquisition system and presented on the display screen, allowing for the real-time assessment of the experiment's progress, and in determining the time for ending the experiment.

6. Results and discussions

This section presents the gathered footing load–settlement results in the form of bearing pressure–

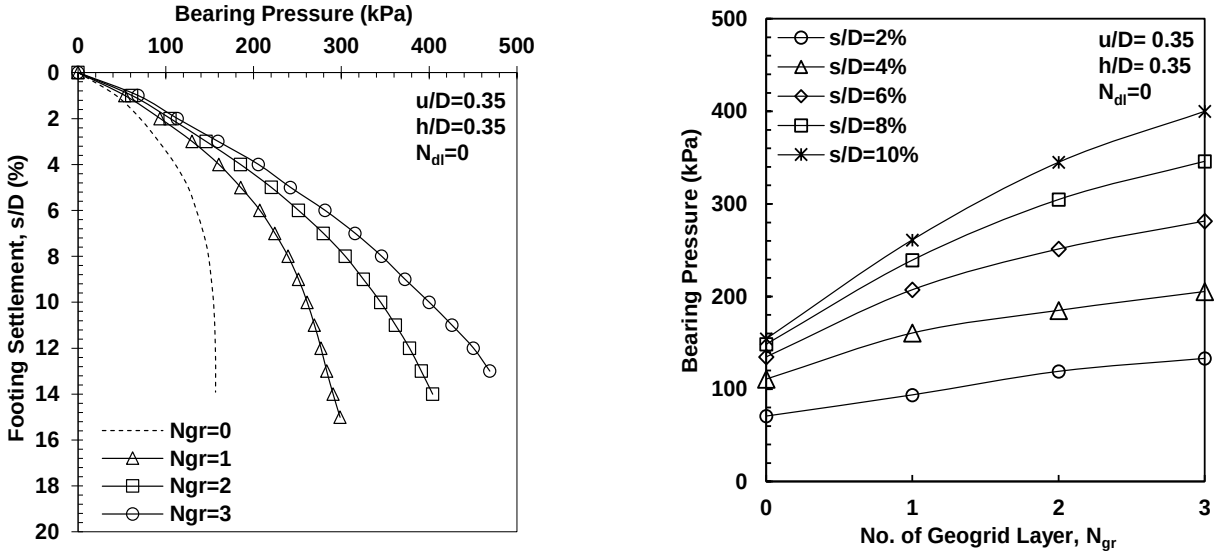

Fig. 5 Variation of bearing pressure resistance for unreinforced and geogrid-reinforced sand beds as functions of (a) footing settlement ratio and (b) number of geogrid layers

settlement ratio plots. Here the settlement ratio is defined as the ratio of the measured settlement (s) to the footing diameter, expressed as a percentage (i.e., $s\times100/D$). Additionally, the impact of each variable (i.e., N_{gr}, N_{dl} and T_l) on the bearing pressure resistances mobilized at specific settlement ratios is examined in terms of an improvement factor (*IF*). It should be noted that, in many studies on the bearing capacity of footings, performance is often evaluated based on bearing capacity alone, without considering the settlement limit criterion (e.g., Dash *et al.* 2003, Sireesh *et al.* 2009). Practical design, however, is often governed by settlement rather than bearing capacity. Improvement in bearing capacity due to reinforcement is frequently estimated at high settlement levels (40%-50% of footing width) or even in ultimate bearing capacity, which are unrealistic for practical designs (e.g., Dash *et al.* 2003, Sitharam *et al.* 2009). In this study, the focus of performance improvement through reinforcement is to enhance bearing capacity for settlements that are less than 10% of the footing width.

6.1 Effect of geogrid reinforcement layers (N_{gr} = 1–3, N_{dl} = 0)

Fig. 5(a) shows the bearing pressure–settlement relationships for the unreinforced sand bed and the geogrid-reinforced sand beds with one, two or three geogrid layers (i.e., without densified SwG layer(s)). As expected, the bearing pressure resistance increased for increasing footing settlement. However, compared to the unreinforced sand bed, the geogrid-reinforced sand beds had considerably stiffer responses — greater stiffness being delivered for more geogrid layers — such that the bearing pressure resistance increases for a given footing settlement ratio. For instance, the unreinforced sand bed mobilized an ultimate (peak) bearing capacity of 157 kPa for s/D = 12%, whereas the bearing pressure resistances mobilized for the geogrid-reinforced sand beds were still continuing to increase on termination of these tests (at $s/D \approx 14\%$). One of the beneficial actions of the geogrid layers is a "tensioned membrane" effect, with further tension force mobilized along the geogrid's length as the rut depth in the deformed geogrid layer increases (Guo *et al.* 2020). The vertical component of this tension force mobilized within the reinforcement layers plays a beneficial role in reducing the stresses exerted on the underlying soil layer(s). Consequently, it leads to an increase in the footing's bearing capacity and reduced deformation or settlement of the foundation bed.

Fig. 5(b) shows the variation in bearing pressure resistances with the number of geogrid layers for different footing settlement ratios (of s/D = 2%, 4%, 6%, 8% and 10%). Note, the value of s/D = 10% is often taken as a limiting condition (Gavin et al. 2009). Considering an s/D of 4%, the bearing pressure resistance of the unreinforced sand bed is 111 kPa, whereas it increased to 161, 185 and 205 kPa for the sand beds reinforced with one, two and three geogrid layers, respectively. However, despite the bearing pressure resistance increasing for more geogrid layers present, it is observed from Fig. 5(b) that compared to large settlement ratio values, the proportional increases in the bearing pressure resistance occur at lesser rates for the low range of settlement ratios generally tolerable and allowable in practice. The latter behavior can be simply explained by the small geogrid deformation/strain developed for small footing settlements, and with less tensile force mobilized along the geogrid's length, the "tensioned membrane" effect is also small. Furthermore, considering a given s/D level, the proportional increase in the bearing pressure resistance reduces somewhat for more geogrid layers present, particularly in moving from N_{gr} = 2 to 3.

The role of the geogrid reinforcement in improving the footing's bearing pressure resistance is further explored

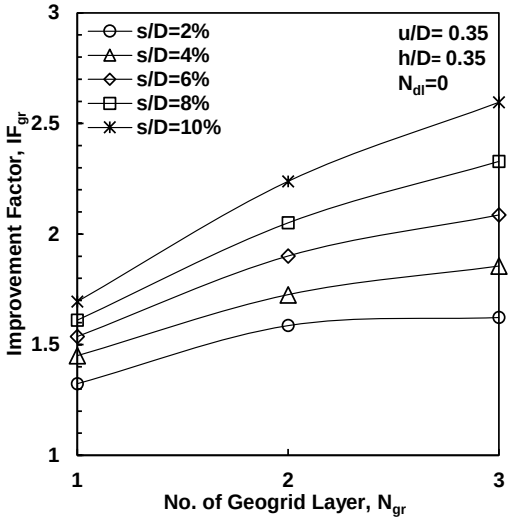

Fig. 6 Variations of IF_{gr} with number of geogrid layers considering different footing settlement ratios

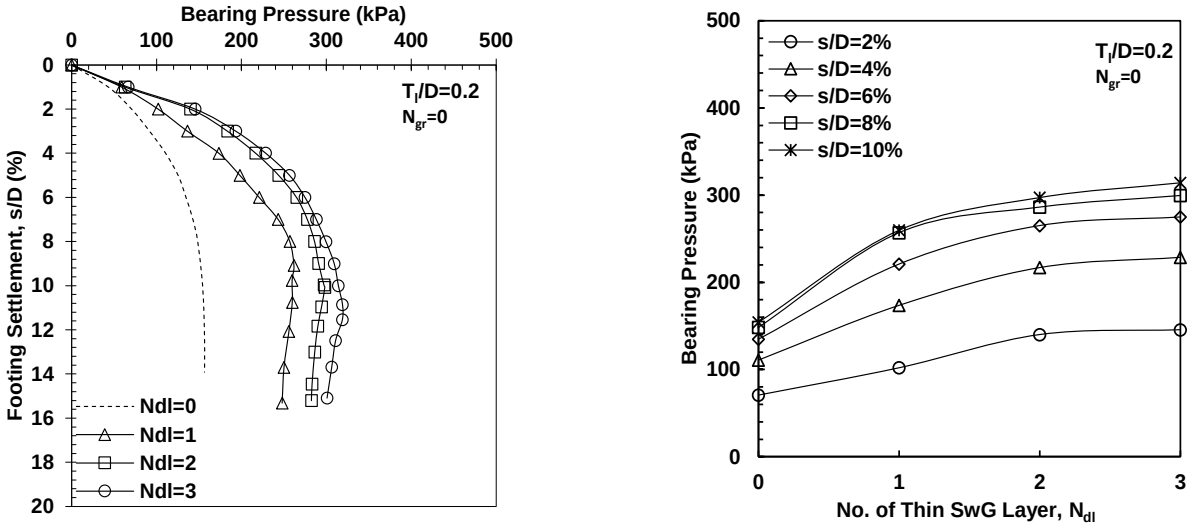

(a) (b)

Fig. 7 Unreinforced sand bed and sand beds incorporating thin densified SwG layers showing variations of bearing pressure resistance with (a) footing settlement ratio and (b) number of SwG layers

considering a given footing settlement (ratio) using a non-dimensional IF (i.e., IF_{gr}), which gives the ratio of the bearing pressures mobilised for the geogrid-reinforcement sand beds (considering N_{gr} = 1, 2 and 3) to that mobilized for the unreinforced sand bed (Eq. (1)).

$$IF_{gr} = p_{gr}/p_{ur} \quad (1)$$

where p_{ur} and p_{gr} are the bearing pressure values mobilized at a given settlement ratio for the unreinforced and geogrid-reinforced sand beds, respectively.

The variation of IF_{gr} with N_{gr}, considering different settlement ratios of s/D = 2%, 4%, 6%, 8% and 10%, is presented in Fig. 6. Again, it is observed that the overall enhancement in the bearing pressure (IF_{gr}) increased for increasing N_{gr} (from 1 to 3). Similarly, the rate of IF_{gr} enhancement with increasing N_{gr} was smaller at low footing settlement ratio values, and the enhancement rate was observed to further reduce for N_{gr} increasing from 2 to 3. For instance, considering an s/D value of 2%, compared to the unreinforced condition there were 32%, 58% and 62% increases in the bearing capacity resistance (i.e., IF_{gr} = 1.32, 1.58 and 1.62) for incorporating one, two and three geogrid layers, respectively, in the sand beds. This example suggests that for low settlement ratio values, the use of a fourth layer (and even using a third layer) of geogrid reinforcement in the sand beds would not produce significant additional improvements in the bearing capacity resistance. This can be attributed to the considerable vertical distance between the footing (at the sand bed surface) and an embedded fourth geogrid layer, with the latter locating below the footing's stress influence zone. Note the footing's stress influence zone has a relatively shallow depth because of the medium-dense state and hence relatively low friction angle (with ϕ = 32.5° measured in triaxial compression) of the placed sand layers.

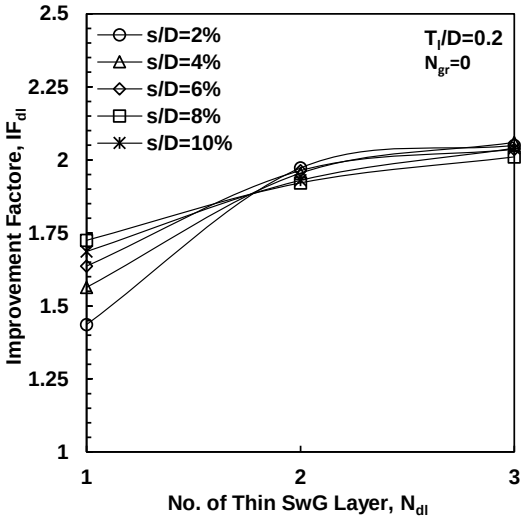

Fig. 8 Variations of IF_{dl} with number of thin densified SwG layers considering different footing settlement ratios

6.2 Effect of thin densified SwG layers (i.e., N_{gr} = 0, N_{dl} = 1–3, T_l/D = 0.20)

Fig. 7(a) shows the bearing pressure–settlement relationships for the sand beds incorporating one, two or three thin densified SwG layers, each 30-mm in thickness (i.e., T_l = 30 mm $\Rightarrow$ T_l/D = 0.20), and with no geogrid layer included in the densified layers. As observed, compared to the unreinforced sand bed, the inclusion of the densified SwG layers within the sand beds noticeable changed the footing's bearing pressure–settlement behavior, with substantially improved bearing pressure resistances, and their peak bearing capacities mobilized for s/D = 10–12%. The bearing pressure resistance improvements achieved for increasing N_{dl} can be simply explained by the substitution of a portion(s) of the medium-dense sand beds with densified SwG material (ϕ = 32.5° and 37.5°, respectively), thereby producing an overall improved friction angle and higher shear resistance within the footing's stress influence zone.

Fig. 7(b) shows the variation in bearing pressure resistances with N_{dl} for different footing settlement ratios. Although the bearing pressure resistance increases for more densified layers, it is observed from Fig. 7(b) that smaller rates of increase occur for the lower range of settlement ratios plotted. Furthermore, considering a given s/D level, relatively small proportional increases in the bearing pressure resistance occur for going from N_{dl} = 2 to 3 densified layers. For instance, considering an s/D value of 2%, the bearing pressure resistances for the sand beds with N_{dl} = 0, 1, 2 and 3 layers are 71, 102, 140 and 146 kPa, respectively. In other words, for small footing settlements, compared to the case with two densified SwG layers, the inclusion of the third densified layer in the sand bed did not produce a significant further improvement in the bearing capacity resistance. Again, this can be simply explained by the third (lowermost) densified SwG layer being located below the footing's zone of significant stress influence, with greater dissipation of the applied footing stress with depth occurring because of the reinforcing effect of the shallower (first and second) densified SwG layers. Based on these results, it can be expected that the inclusion of a fourth densified layer (and even using a third densified layer) would not produce significant additional improvements in the bearing capacity resistance.

The role of the thin densified SwG layers in improving the footing's bearing pressure resistance is further explored for a given footing settlement (ratio) using the IF_{dl} parameter, which gives the ratio of the bearing pressures mobilised for the sand beds incorporating the unreinforced densified SwG layers to that mobilized by the unreinforced sand bed (Eq. (2)).

$$IF_{dl} = p_{dl}/p_{ur} \tag{2}$$

where p_{ur} and p_{dl} are the bearing pressure values mobilized at a given settlement ratio for the unreinforced sand bed and the sand beds incorporating thin densified SwG layers, respectively.

The variation of IF_{dl} with N_{dl}, considering different settlement ratios of s/D = 2%, 4%, 6%, 8% and 10%, is presented in Fig. 8. It is observed that the enhancement in IF_{dl} increased significantly for increasing N_{dl} from 1 to 2, with greater rates of IF_{dl} gain occurring for low footing settlement ratio values, although the enhancement rate is seen to dramatically reduce overall for N_{dl} increasing from 2 to 3. For instance, considering an s/D value of 2%, compared to the unreinforced condition, there were 44%, 97% and 105% increases in the bearing capacity resistances for incorporating one, two and three thin densified SwG layers, respectively, in the sand beds. In other words, the inclusion of two densified SwG layers in the sand beds approximately doubled the bearing pressure resistance, but the inclusion of the third (or more) SwG layer did not produce significant additional improvement in the bearing capacity resistance.

6.3 Effect of geogrid-reinforced thin densified SwG layers (i.e., $N_{gr\text{-}dl}$ = 1–3, T_l/D = 0.20)

Fig. 9 shows the variation in the bearing pressure

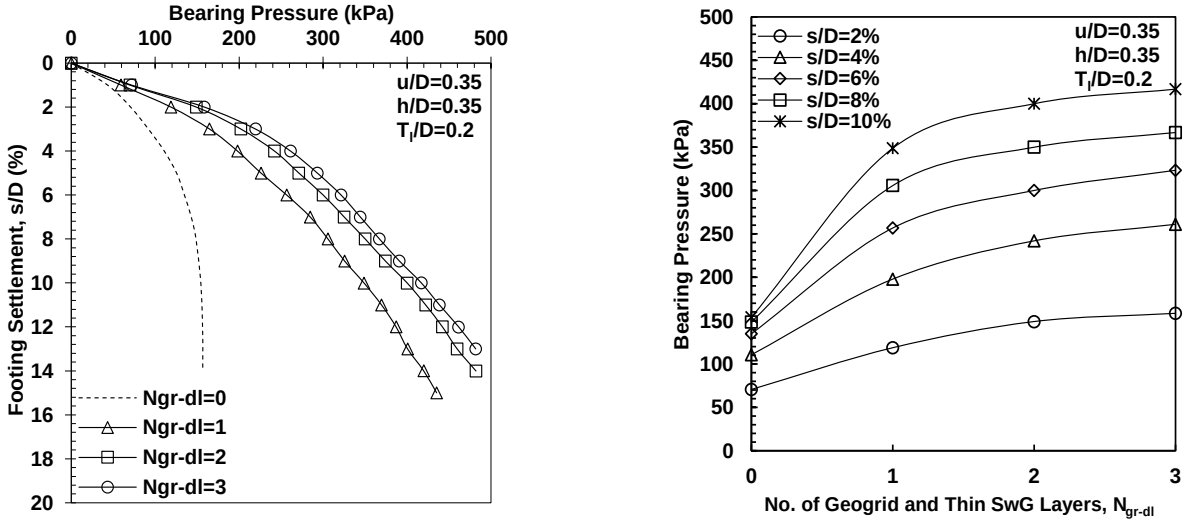

(a) (b)

Fig. 9 Unreinforced sand bed and sand beds incorporating geogrid-reinforced thin densified SwG layers showing variations of bearing pressure resistance with (a) footing settlement ratio and (b) number of geogrid-reinforced SwG layers

resistances relating to the footing settlement ratio for both the unreinforced sand bed and the sand beds reinforced with a geogrid layer encapsulated at the mid-height of thin densified SwG layers incorporated in the sand beds (i.e., $N_{gr\text{-}dl}$ = 1, 2 and 3; see Fig. 4 for the case of $N_{gr\text{-}dl}$ = 3). As observed, considering a specific settlement ratio, the bearing pressure resistance shows significant enhancements with an increase in the number of geogrid-reinforced densified SwG layers. For instance, considering an s/D value of 4%, the bearing pressure resistance increases from 111 kPa for the unreinforced sand bed to 198, 242 and 261 kPa for inclusion of one, two and three geogrid-reinforced thin densified SwG layers, respectively. Moreover, similar to the geogrid-reinforced sand beds (see Fig. 5), the bearing pressure resistances mobilized for the sand beds with geogrid-reinforced densified SwG layers were still continuing to increase on termination of these tests (at $s/D \approx$ 14%). For example, considering the sand bed incorporating a single geogrid-reinforced densified SwG layer, bearing pressure resistances of 119, 198, 257, 306 and 349 kPa were mobilized at settlement ratios of 2%, 4%, 6%, 8% and 10%, respectively. The reasons for these behaviors are that an increase in the footing settlement (a) produces an increase in the rutting depth for the geogrid layer, thereby mobilizing a larger "tensioned membrane" resistance effect, and (b) enhanced interaction/interlock (shearing resistance) between the geogrid reinforcement and SwG particles of the densified layer (as compared to the geogrid reinforcement alone placed in the medium-dense sand beds).

Fig. 10 presents the variation of the IF (i.e., $IF_{gr\text{-}dl}$ given by Eq. (3)) associated with incorporating one, two or three geogrid-reinforced thin densified SwG layers within the medium-dense sand beds, considering different settlement ratios of s/D = 2%, 4%, 6%, 8% and 10%.

$$IF_{gr\text{-}dl} = p_{gr+dl}/p_{ur} \quad (3)$$

where p_{ur} and p_{gr+dl} are the bearing pressure values mobilized at a given settlement ratio for the unreinforced sand bed and the sand beds incorporating geogrid-reinforced densified SwG layers, respectively.

As can be observed from Fig. 10, compared to the unreinforced sand bed, the inclusion of the geogrid-reinforced thin densified SwG layers produced significant increases in the bearing pressure resistance of between 68% (i.e., $IF_{gr\text{-}dl}$ = 1.68 for one geogrid-reinforced densified layer at s/D = 2%) and 170% ($IF_{gr\text{-}dl}$ = 2.70 for three geogrid-reinforced densified layers at s/D = 10%). Moreover, similar to IF_{gr} and IF_{dl}, it is observed from Fig. 10 that the enhancements in $IF_{gr\text{-}dl}$ were proportionately greater for increasing the number of geogrid-reinforced densified layers from 1 to 2 (as compared with from 2 to 3). In other words, Fig. 10 demonstrates that the rate of enhancement in $IF_{gr\text{-}dl}$ decreases with an increase in the number of geogrid-reinforced thin densified SwG layers. Performance improvement becomes almost insignificant beyond three $N_{gr\text{-}dl}$, therefore, the use of four layers of the geogrid-reinforced thin densified SwG is not applicable.

6.4 Performance comparisons for geogrid reinforcement, densified SwG layer and their combinations considering the case of T_l/D = 0.20

In order to better understand the relative performances of the geogrid reinforcement, thin densified SwG layer and combined geogrid-reinforced densified SwG layer inclusions for improving the footing's bearing pressure resistance, Fig. 11 illustrates the variations of their IF values (i.e., IF_{gr}, IF_{dl} and $IF_{gr\text{-}dl}$) with the associated number of layers (i.e., N_{gr}, N_{dl} and $N_{gr\text{-}dl}$), considering the settlement ratios of s/D = 2%, 4%, 6% and 8% separately. As observed, for any given settlement ratio value, the combined geogrid-reinforced thin densified SwG layer inclusions provide greater bearing capacity resistance

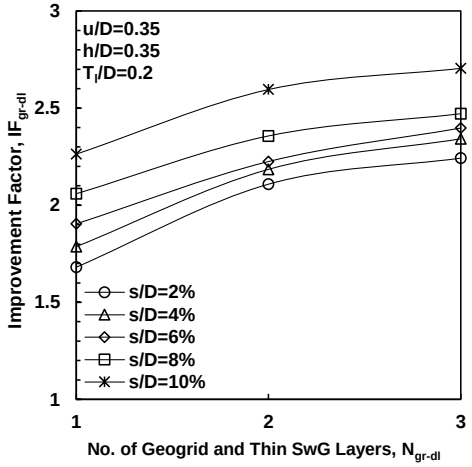

Fig. 10 Variations of $IF_{\text{gr-dl}}$ with number of geogrid-reinforced thin densified SwG layers considering different footing settlement ratios (T_l/D = 0.20)

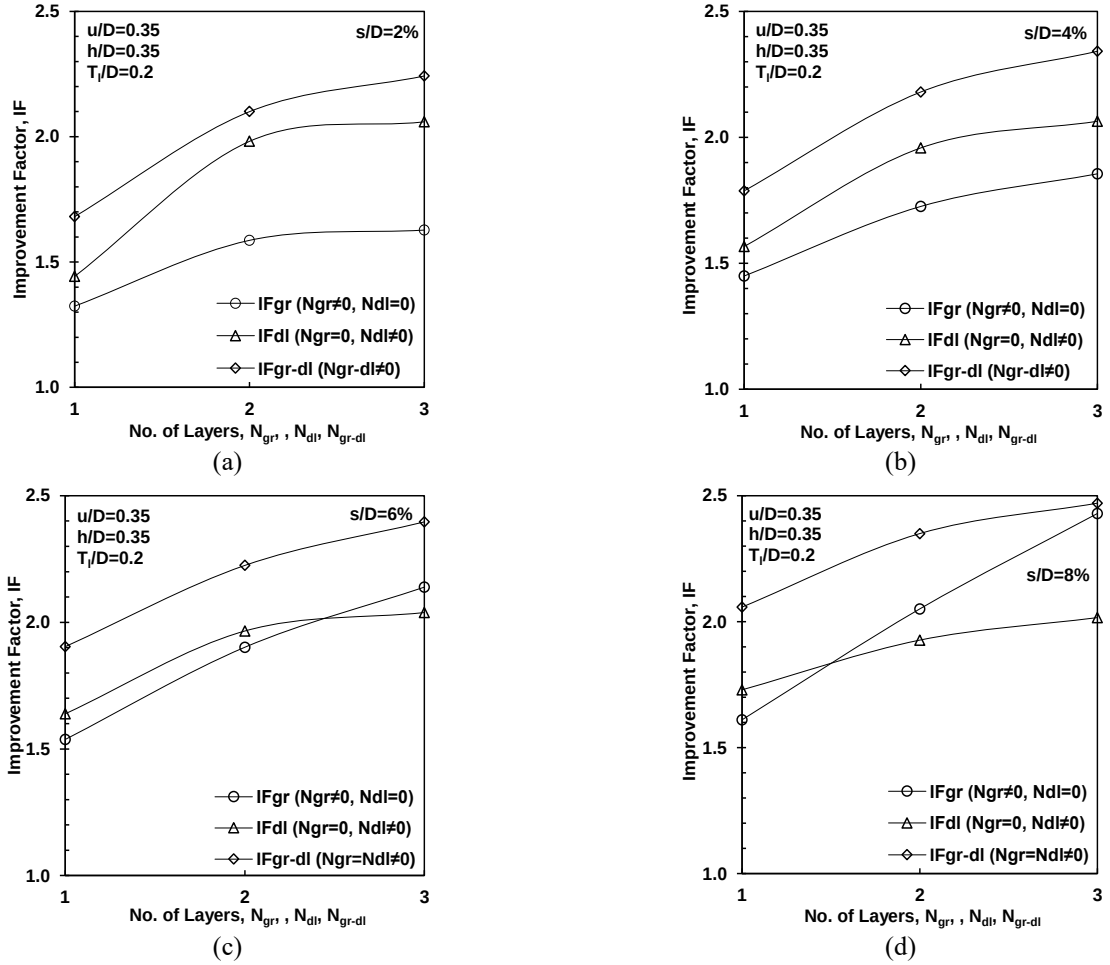

Fig. 11 Variation of the improvement factors IF_{gr}, IF_{dl} and $IF_{\text{gr-dl}}$ with the number of geogrid reinforcement layers (N_{gr}), thin densified SwG layers (N_{dl}) and combined geogrid-reinforced thin densified SwG layers ($N_{\text{gr-dl}}$) considering different footing settlement ratios of s/D = (a) 2%, (b) 4%, (c) 6% and (d) 8%

improvement compared to the cases with either the geogrid reinforcement layers or the unreinforced densified SwG layers. For example, in the cases of two geogrid layers (N_{gr} = 2), two densified SwG layers (N_{dl} = 2) and two geogrid-reinforced densified SwG layers ($N_{\text{gr-dl}}$ = 2), the values of IF_{gr}, IF_{dl} and $IF_{\text{gr-dl}}$ achieved for a settlement ratio of s/D = 4% are 1.72, 1.96 and 2.18, respectively (Fig. 11(b)), i.e., corresponding to bearing pressure resistance improvements of 72%, 96%, and 118%, respectively.

Furthermore, comparing the cases of the two geogrid-

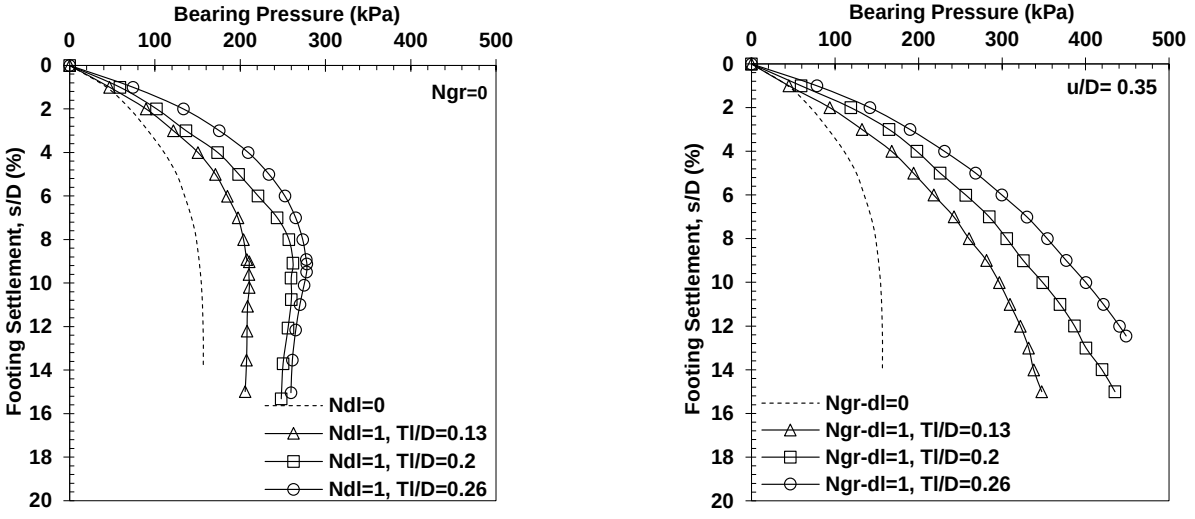

(a) (b)

Fig. 12 Effect of thickness of single densified SwG layer on variation of bearing pressure resistance with footing settlement ratio for (a) unreinforced and (b) geogrid-reinforced SwG layer cases

reinforcement layers (IF_{gr} = 1.72) and the two geogrid-reinforced densified SwG layers ($IF_{gr\text{-}dl}$ = 2.18), the inclusion of the two 30-mm thick densified SwG layers (i.e., T_l/D = 0.2) for the latter case produced a 46% greater bearing pressure resistance. This increased bearing pressure resistance is explained as follows. Firstly, as theoretical expressions for footings on layered systems suggest (Biswas and Murali Krishna 2019, Avesani Neto 2019), substituting the medium-dense uniform sand with the densified SwG can increase the bearing pressure resistance. Even a thin densified SwG layer could influence the test results, and this effect would be enhanced for an increase in the number and thickness of the SwG layers. Secondly, compared to the pullout resistance of the geogrid reinforcement embedded in the medium-dense sand beds, the pullout resistance for embedment in the densified well-graded SwG layers is superior on account of the higher mobilized shear interface strength, which in turn positively influences the footing's bearing capacity resistance.

As observed in Figs. 11(a) and 11(b), at settlement ratios of 2% and 4%, the performances of the foundation beds incorporating the thin densified SwG layers alone is better than those with the geogrid reinforcement alone (i.e., $IF_{dl} > IF_{gr}$). However, for the foundation beds at settlement ratios of 6% and 8% (Figs. 11(c) and 11(d)), the inclusion of the geogrid reinforcement layers alone sometimes (i.e., for the cases of using three geogrid layers at s/D = 6% and using two or three geogrid layers at s/D = 8%) exhibits better performance compared to that achieved for incorporating the densified SwG layers alone. The reason behind this is the strain-level-dependency of the tensile force mobilization along the geogrid reinforcement. In fact, for settlement ratios where the equivalent settlement of the model is equal to or less than s/D of 4%, insufficient tensile force is generated in the geogrid reinforcement due to not enough straining of the reinforcement layers, with insufficient interaction occurring between their upper and lower surfaces and the contacting sand bedding. To better examine the performance mechanism and the influence of the geogrid reinforcement on improving the behavior of the foundation bed, future studies could instrument the geogrid reinforcement using strain gauges for direct measurement of the tensile strain and resulting force acting along the embedded geogrid layers.

6.5 Effect of the densified SwG layer thickness

Figs. 12(a) and 12(b) shows the influence of the SwG layer thickness on the mobilized bearing pressure resistance for the cases of a single densified SwG layer or a single geogrid-reinforced densified SwG layer incorporated in the medium-dense sand beds, investigating SwG layer thicknesses of 20, 30 and 40 mm (i.e., T_l/D = 0.13, 0.20 and 0.26, respectively). As apparent from Fig. 12(a), the peak bearing pressure resistances for the unreinforced densified SwG layers occur at settlement ratios of 9–10%, compared to ~12% for the unreinforced sand bed. However, with the geogrid reinforcement encapsulated within the densified SwG layers, the bearing pressure resistances are seen to monotonically increase for increasing footing settlement ratio (Fig. 12(b)). Furthermore, for both the unreinforced and geogrid-reinforced cases, greater bearing pressure resistances are mobilized for thicker densified SwG layers.

Fig. 13 illustrates the variations of bearing pressure resistance with the thickness of the unreinforced and geogrid-reinforced SwG layers considering different footing settlement ratios of s/D = 2%, 4%, 6% and 8%. According to this figure, in almost all cases the proportional increase in the bearing pressure resistance due to an increase in the SwG layer thickness from 30 to 40 mm (i.e., for T_l/D increasing from 0.20 to 0.26) is marginally greater than that occurs for increasing the SwG layer thickness from 20 to 30 mm (T_l/D from 0.13 to 0.20). With the mid-height of the unreinforced and geogrid-reinforced densified SwG layers all located at the same depth ratio of u/D = 0.33 below the sand bed surface (refer to Fig. 4), increasing the SwG layer

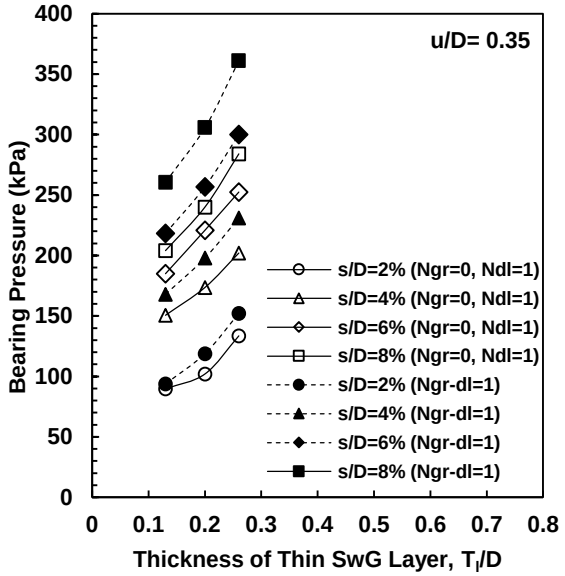

Fig. 13 Variations of bearing pressure resistance with thickness (T_l/D) for single unreinforced and geogrid-reinforced densified SwG layer incorporated in the sand beds, with consideration of different footing settlement ratios (u/D = 0.33)

thickness leads to the replacement of larger portions of the medium-dense uniform sand (with densified coarser material of SwG) in the footing's zone of significant stress influence. This results in an overall improvement in the shear resistance of the soil located beneath the footing, thereby producing a higher bearing pressure resistance. It is evident that further increases in the SwG layer thickness would enhance the bearing pressure resistance even more, with T_l/D = 0.66 representing the limiting condition of completely replacing the medium-dense sand located above and between the incorporated densified SwG layers. However, this goes against the philosophy of using *thin* densified SwG layers and would undoubtedly raise concerns about the economic feasibility of the ground improvement approach in geotechnical engineering practice. Comparative investigations in Fig. 13 suggest that achieving a specified improvement in bearing pressure resistance may involve two possible alternatives. For instance, considering a footing settlement ratio of s/D = 4%, it is found that that sand beds incorporating a 40-mm thick unreinforced densified SwG layer (i.e., T_l/D = 0.26) or a 30-mm thick geogrid-reinforced densified SwG layer (T_l/D = 0.20) produce similar bearing pressure resistances of ~200 kPa. However, the chosen solution entails practical and economic considerations, contingent on factors including the availability of suitable soil material for constructing the SwG layers, the cost of the geogrid reinforcement material, the depth and width of the reinforcement zone beneath the footing (including associated excavation and backfilling costs), and any variations in the soil backfill material and procedures.

7. Relating the model test results to the large-scale condition

Adams and Collin (1997) and Milligan *et al.* (1986) – who studied the small- and large-scale behaviors of granular layers that included geogrid reinforcement – have shown that the fundamental governing mechanisms and observed behaviors in the large-scale tests can be reproduced using model tests. Thus, there can be some confidence that the pattern of results presented herein for the model footing tests will be similar for real full-scale conditions. Nevertheless, it would be wise to perform larger-scale tests, including investigations for different footing shapes, soil types and geogrid reinforcement, to name a few, in further validating the presented model results. The remainder of this section presents a preliminary dimensional analysis aimed at relating the results for the model footing of diameter D_M with a prototype circular footing of diameter D_P that is λ times greater (with the subscripts P and M referring to the prototype and model, respectively)..

In this dimensional analysis, the proposed function for scale analysis should govern the relevant parameters. These are the properties of the sand and SwG soils (i.e., their mean particle sizes D_{50}, unit weights γ, internal friction angles ϕ and shear moduli G, the relative density D_r of the sand beds and relative compaction R_c of the thin densified SwG layers), the geometry and properties of the geogrid reinforcement layers (i.e., their burial depth u, width b, layer spacing h, and reinforcement stiffness J), the thickness T_l of the thin densified layers and the loading conditions (i.e., for a footing diameter D, settlement s and bearing pressure p). Note, the reinforcement stiffness is defined as $J = E_r \times t$, where E_r and t are the Young's modulus and thickness of the geogrid reinforcement elements, respectively. Therefore, the function f that governs the reinforced system can be expressed as follows

$$f(D, u, b, h, D_{50}, s, G, T_l, J, p, \gamma, \phi, D_r, R_c) = 0 \qquad (4)$$

As written, the governing function contains 14 parameters involving two dimensions (i.e., length and force), such that 12 dimensionless parameters can be inferred, as listed in

Eq. (5).

$$g(\pi_1, \pi_2, \pi_3, \ldots, \pi_{12}) = g\left(\frac{u}{D}, \frac{b}{D}, \frac{h}{D}, \frac{D_{50}}{D}, \frac{s}{D}, \frac{T_l}{D}, \frac{G}{\gamma D}, \frac{J}{GD}, \frac{p}{\gamma D}, D_r, R_c, \phi\right) = 0 \quad (5)$$

where g is a function that governs the dimensionless parameters (i.e., π_1, π_2, π_3, …, π_{12}) of the system.

Consider a prototype circular footing with a diameter of D_P that is λ times larger than the model footing having a diameter of D_M (with the subscripts P and M referring to the prototype and model, respectively). The similarity condition should be satisfied for all π_i values (i.e., $(\pi_i)_P = (\pi_i)_M$), as i varies from 1 to 12. Thus, with $D_P = \lambda D_M$ for i = 1 to 6, we can write the following

$$\frac{u_P}{u_M} = \frac{b_P}{b_M} = \frac{h_P}{h_M} = \frac{(D_{50})_P}{(D_{50})_M} = \frac{s_P}{s_M} = \frac{(T_l)_P}{(T_l)_M} = \lambda \quad (6)$$

In other words, the mean particle sizes (D_{50}) of the materials comprising the uniform granular deposit and incorporated thin coarse densified layers for the prototype would be λ times greater than those of the medium sand and SwG materials, respectively, used in the model tests.

Assuming the same soil densities in the prototype and model, other similarity conditions for i = 7, 8 and 9 dictate the following

$$G_P/G_M = p_P/p_M = \lambda \quad (7)$$

$$J_P/J_M = \lambda^2 \quad (8)$$

In other words, the shear modulus values of the materials comprising the uniform granular deposit and incorporated thin coarse densified layers should be λ times those of the medium sand and SwG materials used at model-scale, whereas the geogrid reinforcement stiffness J for the prototype should be λ^2 times greater than that used in the model tests. If the above conditions are satisfied, then for a given footing settlement the bearing pressure mobilized for the prototype is expected to be λ times the bearing pressure resistance achieved in the model study.

Considering the diameter dimension of the model footing (i.e., D_M = 150 mm), the value of λ for many practical applications is likely to range from 1 to 7 (e.g., $\lambda \approx$ 1 and 7 would typically apply for a truck tire and a 1-m diameter footing, respectively), implying that 1–7 fold increases in the soil D_{50} values and a 1–50 fold increase in the reinforcement stiffness are required. As an example, going from a model footing diameter of D_M = 150 mm to a full-scale footing diameter of D_P = 750 mm (i.e., λ = 5) requires that the tensile strength mobilized for a given strain of the geosynthetic elements incorporated at full-scale should be 25 (i.e., λ^2) times greater than that used in the model. The geogrid employed in the model tests mobilized tensile resistances of 0.10, 0.58 and 1.43 kN/m at 1%, 5% and 10% strains, respectively. Hence, the equivalent tensile resistances of the reinforcement elements for the prototype would be about 2.5, 14.5 and 35.75 kN/m – which are within the capabilities of available conventional geosynthetics. Moreover, with the uniform sand and SwG materials having D_{50} values of 1.2 and 2.3 mm, respectively, the D_{50} of the uniform soil and coarser material comprising the uniform beds and densified layers of the prototype would be 6.0 and 11.5 mm, respectively. In addition, if the thickness of the thin sand layers between the densified SwG layers used in the model tests is $h - T_l$ = 30 mm, it should increase to 150 mm for the porotype.

8. Conclusions

The model foundation testing presented herein investigated the effects of incorporating one, two and three separate geogrid-reinforced thin densified SwG layers on the bearing pressure resistance improvement for medium-dense uniform sand beds when subjected to monotonic vertical loading of a circular footing placed on the sand bed surface. The levels of improvement achieved were assessed relative to the bearing pressure resistances mobilized for (a) unreinforced, (b) geogrid-reinforced, and (c) thin densified SwG-layer-reinforced sand beds. Overall, the presented experimental results have qualitatively provided a useful perspective on the basic mechanisms responsible for the bearing pressure resistance versus settlement behaviors. The pertinent conclusions are summarized, as follows:

- Compared to the unreinforced sand bed, the foundation beds with geogrid reinforcement, thin densified SwG layer or geogrid-reinforced thin densified SwG layer inclusions produced significantly stiffer responses and mobilized greater bearing pressure resistances, with the best performance obtained for the geogrid-reinforced thin densified SwG layer inclusions.
- For sand beds incorporating geogrid reinforcement and geogrid-reinforced densified SwG layers, the mobilized bearing pressure resistances continued to increase for s/D > 10% due to the intensifying tension force developed along the geogrid's length for increasing rut depth in the deformed geogrid layer. Additionally, for geogrid-reinforced densified SwG layers, along with producing superior interface shear resistance mobilized between the geogrid and SwG particles, the substitution of portions of the medium-dense sand beds with densified SwG layers of higher internal friction angle delivered better overall shearing resistance within the footing's stress influence zone.
- Increasing the number of geogrid reinforcement, densified SwG and geogrid-reinforced densified SwG layer inclusions from one to three produced superior geomechanical performance. However, the proportional performance improvement reduced for including more layers, with the introduction of a fourth layer not expected to produce significant additional performance benefits, simply because the fourth introduced layer would locate below the footing's stress influence zone.
- Increasing the SwG layer thickness leads to greater bearing pressure resistances, simply because larger portions of the medium-dense uniform sand located within the footing's zone of significant stress influence are replaced with densified SwG material having a higher shearing resistance. However, large increases in

the SwG layer thickness would go against the philosophy of using *thin* densified SwG layers and would undoubtedly raise concerns about the economic feasibility of the ground improvement approach in geotechnical engineering practice.

It is recommended that larger-scale experiments (including investigations of different footing shapes, as well as soil and geogrid types) be performed to validate the presented findings, along with examining the associated scale effects. In this regard, our experimental study provides a useful basis for designing future larger-scale studies and for simulation with numerical models. Furthermore, future studies could instrument the embedded geogrid reinforcement layers to obtain direct measurements of the acting soil pressures and reinforcement strains, thereby providing additional results for understanding the mechanisms of improved bearing capacity resistance. Additionally, although the tests were performed under monotonic loading, the general findings can be applicable to roads and pavements subjected to traffic loads (repeated loading). However, similar tests under repeated loading are recommended to investigate the performance of geogrid-reinforced thin densified SwG layers on the settlement response of medium-dense uniform sand beds in future studies.

References

Abdi, M.R. and Arjomand, M.A. (2011), "Pullout tests conducted on clay reinforced with geogrid encapsulated in thin layers of sand", *Geotext. Geomembranes*, **29**(6), 588-595. https://doi.org/10.1016/j.geotexmem.2011.04.004.

Abdi, M.R., Sadrnejad, A. and Arjomand, M.A. (2009), "Strength enhancement of clay by encapsulating geogrids in thin layers of sand", *Geotext. Geomembranes*, **27**(6), 447-455. https://doi.org/10.1016/j.geotexmem.2009.06.001.

Abdi, M.R. and Zandieh, A.R. (2014), "Experimental and numerical analysis of large scale pull out tests conducted on clays reinforced with geogrids encapsulated with coarse material", *Geotext. Geomembranes*, **42**(5), 494-504. https://doi.org/10.1016/j.geotexmem.2014.07.008.

Abdi, M.R., Zandieh, A., Mirzaeifar, H. and Arjomand, M.A. (2019), "Influence of geogrid type and coarse grain size on pull out behaviour of clays reinforced with geogrids embedded in thin granular layers", *Eur. J. Environ. Civil Eng*., 2161-2180. https://doi.org/10.1080/19648189.2019.1619627.

Adams, M.T. and Collin, J.G. (1997), "Large model spread footing load tests on geosynthetic reinforced soil foundations", *J. Geotech. Geoenviron. Eng*., **123**(1), 66-72. https://doi.org/10.1061/(ASCE)1090-0241(1997)123:1(66).

Ahmadian, A.F. and Moghaddas Tafreshi, S.N. (2020), "Experimental investigation of the behavior of sand-EPS beads mixure reinforced by geotextile layers encapsulated with lens layers", *Sharif J. Civil Eng*., **36.2**(1-1), 57-68. https://sid.ir/paper/961994/en.

ASTM D1557-12. (2012), Standard Test Methods for Laboratory Compaction Characteristics of Soil Using Modified Effort. ASTM International, West Conshohocken, PA, USA. https://doi.org/10.1520/D1557-12R21.

Altay, G., Kayadelen, C., Çanakci, H., Bagriacik, B., Ok, B. and Oguzhanoglu, M.A. (2021), Experimental investigation of deformation behavior of geocell retaining walls", *Geomech. Eng*., **27**(5), 419-431. https://doi.org/10.12989/gae.2021.27.5.419.

Avesani Neto, J.O. (2019), "Application of the two-layer system theory to calculate the settlements and vertical stress propagation in soil reinforcement with geocell", *Geotext. Geomembranes*, **47**(1), 32-41. https://doi.org/10.1016/j.geotexmem.2018.09.003.

Biswas, S. and Mittal, S. (2017), "Square footing on geocell reinforced cohesionless soils", *Geomech. Eng*., **13**(4), 641-651. https://doi.org/10.12989/gae.2017.13.4.641.

Biswas, A. and Krishna, A.M. (2018), "Behaviour of geocell–geogrid reinforced foundations on clay subgrades of varying strengths", *Int. J. Phys. Model. Geotech*., **18**(6), 301-314. https://doi.org/10.1680/jphmg.17.00013.

Biswas, A. and Krishna, A.M. (2019), "Behaviour of circular footing resting on layered foundation: sand overlying clay of varying strengths", *Int. J. Geotech. Eng*., **13**(1), 9-24, https://doi.org/10.1080/19386362.2017.1314242.

Dash, S.K., Sireesh, S. and Sitharam, T.G. (2003), "Model studies on circular footing supported on geocell reinforced sand underlain by soft clay", *Geotext. Geomembranes*, **21**(4), 197-219. https://doi.org/10.1016/S0266-1144(03)00017-7.

Gavin, K.G., Adekunte, A. and O'Kelly, B.C. (2009), "A field investigation of vertical footing response on sand", *Proceedings of the Institution of Civil Engineers – Geotechnical Engineering*, **162**(5), 257-267. https://doi.org/10.1680/geng.2009.162.5.257.

Ghiassian, H. and Jahannia, M. (2004), "Influence of encapsulated geogrid-sand system on bearing capacity and settlement characteristics of reinforced clay", *Int. J. Civil Eng*., **2**(1), 45-53.

Giroud, J.P., Han, J., Tutumluer, E. and Dobie, M.J.D. (2023), "The use of geosynthetics in roads", *Geosynthetics Int*., **30**(1), 47-80. https://doi.org/10.1680/jgein.21.00046.

Guo, X., Zhang, H. and Liu, L. (2020), "Planar geosynthetic-reinforced soil foundations: A review", *SN Appl. Sci.*, **2**(11), 2074. https://doi.org/10.1007/s42452-020-03930-5.

Khalaj, O., Moghaddas Tafreshi, S.N., Dawson, A.R. and Mašek, B., (2015), "Improvement of pavement foundation response with multi-layers of geocell reinforcement: Cyclic plate load test", *Geomech. Eng*., **9**(3), 373-395. https://doi.org/10.12989/gae.2015.9.3.373.

Liu, J., Zhu, K., Cai, Y., Pang, S. and Sheng, Y. (2024), "Fractional model and deformation of fiber-reinforced soil under traffic loads", *Geomech. Eng*., **39**(2), 143-155. https://doi.org/10.12989/gae.2024.39.2.143.

Liu, W., Xu, P., Yang, G. and Rong, M. (2024), "Seismic stability of MSE walls with stepped reinforcement arrangement subjected to vertical and horizontal accelerations", *Geomech. Eng*., **39**(5), 503-512. https://doi.org/10.12989/gae.2024.39.5.503.

Milligan, GWE., Fannin, RJ. and Farrar., DM. (1986), "Model and full-scale tests of granular layers reinforced with a geogrid", *Proceedings of 3rd International Conference on Geotextiles*, Vienna, Italy.

Moghaddas Tafreshi, S.N. and Dawson, A. (2010), "Behaviour of footings on reinforced sand subjected to repeated loading – Comparing use of 3D and planar geotextile", *Geotext. Geomembranes*, **28**(5), 434-447. https://doi.org/10.1016/j.geotexmem.2009.12.007.

Moghaddas Tafreshi, S.N., Parvizi Omran, M., Rahimi, M. and Dawson, A.R. (2021), "Experimental investigation of the behavior of soil reinforced with waste plastic bottles under cyclic loads", *Transport. Geotech*., **26**, 100455, https://doi.org/10.1016/j.trgeo.2020.100455.

Moghaddas Tafreshi, S.N., Karami, N., Rahimi, M. and Dawson, A.R. (2022), "Response of a model footing reinforced by novel three dimensional elements", *Int. J. Phys. Model. Geotech*.,

23(2), 92-111. https://doi.org/10.1680/jphmg.21.00055.
Ok, B., Colakoglu, H. and Dagli, U. (2023), "Evaluation of the geogrid-various sustainable geomaterials interaction by direct shear tests", *Geomech. Eng*., **34**(2), 173-186. https://doi.org/10.12989/gae.2023.34.2.173.
O'Kelly, B.C. and Naughton, P.J. (2008a), "Enhancement in the interface shear resistance achieved by novel geogrid with in-plane drainage", *Proceedings of the GeoCongress 2008*, New Orleans, Louisiana, USA. GSP 178. ASCE: Reston, VA, USA. https://doi.org/10.1061/40971(310)92.
O'Kelly, B.C. and Naughton P.J. (2008b), "On the interface shear resistance of a novel geogrid with in-plane drainage capability", *Geotext. Geomembranes*, **26**(4), 357-362. https://doi.org/10.1016/j.geotexmem.2007.12.006.
Ouyang, F., Wu, Z., Wang, y., Wang, Z., Cao, J., Wang, K. and Zhang, J. (2024), "Field tests on partially geotextile encased stone column-supported embankment over silty clay", *Geotext. Geomembranes*, **52**(1), 95-109. https://doi.org/10.1016/j.geotexmem.2023.09.005.
Pires, A.C. and Palmeira, E.M. (2021), "The influence of geosynthetic reinforcement on the mechanical behaviour of soil-pipe systems", *Geotext. Geomembranes*, **49**(5), 1117-1128. https://doi.org/10.1016/j.geotexmem.2021.03.006.
Punetha, P. and Nimbalkar, S. (2022), "Performance improvement of ballasted railway tracks using three-dimensional cellular geoinclusions", *Geotext. Geomembranes*, **50**(6), 1061-1082. https://doi.org/10.1016/j.geotexmem.2022.06.007.
Roy, N., Mukherjee, S. and Ghosh, A. (2024), "A study on pullout behavior of plate anchor in reinforced soft clay", *Geomech. Eng.*, **39**(5), 455-474. https://doi.org/10.12989/gae.2024.39.5.455.
Sireesh, S., Sitharam, T. and Dash, S.K. (2009), "Bearing capacity of circular footing on geocell–sand mattress overlying clay bed with void", *Geotext. Geomembranes*, **27**(2), 89-98. https://doi.org/10.1016/j.geotexmem.2008.09.005.
Tarraf, M. and Seyedi Hosseininia, E. (2024), "The exact bearing capacity of strip footings on reinforced slopes using slip line method", *Geomech. Eng*., **38**(3), 261-273. https://doi.org/10.12989/gae.2024.38.3.261.
Tolun, M., Epsileli, S.E., Emirler, B., Yildiz, A. and Tutumluer, E. (2021), "Contribution of using geogrid under a shallow foundation on sand subjected to static and repeated loads: Laboratory testing and numerical simulations", *Geomech. Eng*., **27**(2), 167-178. https://doi.org/10.12989/gae.2021.27.2.167.
Yazdani, H. and Ashtiani, M. (2023), "The behaviour of a strip footing resting on geosynthetics-reinforced slopes", *Geomech. Eng*., **34**(6), 623-636. https://doi.org/10.12989/gae.2023.34.6.623.
Zhao, Y., Lu, Z., Liu, J., Ye, L., Xu, W. and Yao, H. (2023), "Effect of cohesion of infill materials on the performance of geocell-reinforced cohesive soil subgrade", *Geomech. Eng*., **33**(3), 301-315. https://doi.org/10.12989/gae.2023.33.3.301.
Zhao, Y., Lu, Z., Liu, J., Zhang, J., Tang, C. and Yao, H. (2024), "Evolution of pullout behavior of geocell embedded in sandy soil", *Geomech. Eng*., **38**(3), 275-284. https://doi.org/10.12989/gae.2024.38.3.275.

Abbreviations

IF	improvement factor (of bearing pressure resistance)
LVDT	linear-variable displacement transducer
MDF	medium-density fiberboard
MDUW	maximum dry unit weight
MP	modified Proctor (compaction) SwG sand with gravel (soil)

Notations

b	side dimension of embedded square geogrid-reinforcement layer [mm]
C_c	Coefficient of curvature [–]
C_u	Coefficient of uniformity [–]
D	footing diameter [mm]
D_{50}	mean grain size [mm]
D_{10}, D_{30}, D_{60}	Diameter of soil particles at which 10%, 30% and 60% of the sample's mass is comprised of particles with a diameter less than these values, respectively [mm]
D_r	relative density (of sand beds) [%]
E_r	Young's modulus of geogrid reinforcement [**kN/m^2**]
f	function governing the system parameters [–]
g	function governing the dimensionless parameters of the system [–]
G	shear modulus **[kN/m^2]**
G_s	specific gravity of solids [–]
h	vertical spacing between centers of neighboring geogrid layers incorporated in sand beds [mm]
IF_{dl}	bearing pressure improvement factor for sand bed with thin densified SwG layer(s) (= p_{dl}/p_{ur}) [–]
IF_{gr}	bearing pressure improvement factor for geogrid-reinforced sand bed (= p_{gr}/p_{ur}) [–]
$IF_{gr\text{-}dl}$	bearing pressure improvement factor for sand bed with geogrid-reinforced thin densified SwG layer(s) (= p_{gr+dl}/p_{ur}) [–]
J	stiffness of geogrid reinforcement material **[kN/m]**
N_{dl}	number of thin densified SwG layers [–]
N_{gr}	number of geogrid reinforcement layers [–]
$N_{gr\text{-}dl}$	number of geogrid-reinforced densified SwG layers [–]
p	bearing pressure resistance [kPa]
p_{dl}	bearing pressure resistance at given settlement ratio for sand bed with densified SwG layer(s) [kPa]
p_{gr}	bearing pressure resistance at given settlement ratio for geogrid-reinforced sand bed [kPa]
$p_{gr\text{-}dl}$	bearing pressure resistance at given settlement ratio for sand bed with geogrid-reinforced densified SwG layer(s) [kPa]
p_{ur}	bearing pressure resistance at given settlement ratio for unreinforced sand bed [kPa]
R_c	relative compaction (of densified SwG layers) [%]
s	footing settlement [mm]
t	thickness of geogrid reinforcement layer/element [mm]
T_l	thickness of each densified SwG layer [mm]
u	placement depth to center of uppermost geogrid reinforcement layer [mm]
ϕ	internal friction angle [degree]
γ	unit weight *[kN/m^3]*
λ	geometrical proportionality (relating prototype to model) [–]
π_1– π_{12}	Buckingham's dimensionless parameters [–]

Subscripts

P	referring to the prototype (e.g., D_P = prototype footing diameter)
M	referring to the model (e.g., D_M = model footing diameter)